Available online at https://sej.journals.ekb.eg/
FACULTY OF ENGINEERING – SOHAG UNIVERSITY
Sohag Engineering Journal (SEJ) Vol. 3, No. 2, September 2023

Optimal Setting of the Proportional–Integral Controllers for Performance Enhancement of the WECS Based on PMSG Under Grid Faults Using Novel Optimization Algorithm

Abd-Elhady Ramadan[a*], Khairy Sayed [a], Mohamed Ebeed [a,b], Salah Kamel[c], Ahmed Refai[a], Francisco Jurado[b]

[a] *Electrical Engineering Department, Sohag University, 82524, Sohag, Egypt*
[b] *Department of Electrical Engineering, University of Jaén, 23700 EPS Linares, Jaén, Spain.*
[c] *Electrical Engineering Department, Faculty of Engineering, Aswan University, Aswan 81542, Egypt.*

Abstract

Because of the depletion of fossil fuels, as well as economic and environmental concerns, renewable energy resources (RERs) have become widely integrated into the power system. The permanent magnet synchronous generator (PMSG) is regarded as one of the most promising wind energy conversion technologies (WECS). However, if a fault occurs, the PMSG's behavior will be significantly altered. This study describes a new attempt to optimally design proportional-integral (PI) controllers using a novel partial swarm optimization (PSO) approach. All converters of a grid-connected (PMSG) driven by a variable-speed wind turbine use optimal PI controllers. Such WECSs (WECS) include a machine -side converter (MSC) and a grid-side converter (GSC). The proposed PSO-based PI controllers use a vector control technique to optimally control both of these converters. The MSC is employed for determining the maximum power point. generator currents and reactive generated power Furthermore, the GSC is mostly used to regulate the point of common coupling (PCC) voltage, DC -bus voltage, and grid currents. The PSO is used to minimize the fitness function, which has the squared error of the sum of these variables. The range of the proportional and integral gains of the PI controllers is one of the constraints of the optimization problem. MATLAB/SIMULINK software is used to implement all simulation investigated results, including the PSO code. This is a notable and novel contribution of this study, The proposed PSO based PI controllers are validated against a variety of network disturbances, including balanced and unbalanced faults. The grid-linked PMSG's low voltage ride-through ability can be improved even more with the appropriate PSO based PI controllers.

 DOI: 10.21608/SEJ.2023.197730.1033

Keywords: wind turbines; PMSG; WECS; grid faults; three phase to ground fault; line to line fault; PSO optimizer.

Abbreviations			
WECS	Wind energy conversion system	**MSC**	Machine-side converter
VSWT	Variable-speed Wind Turbine	**GSC**	Grid-side converter
FSWT	Fixed-speed Wind Turbine	**PCC**	Common coupling point
PMSG	Permanent magnet synchronous generator	**BTBC**	Back-to-back converter
MPPT	Maximum power point tracking	**FRT**	Fault-ride-through
SCIG	Squirrel cage induction generator	**LVRT**	Low voltage ride through
DFIG	Doubly fed induction generator	**SMC**	Sliding mode controller
ANFIS	Adaptive neuro fuzzy interface system	**PSO**	particle swarm optimizer

List of symbols			
$\mathbf{T_{em}}$	Electromagnetic torque	$\boldsymbol{\psi_f}$	Flux linkage
T	Mechanical torque	**f**	Vicious damping coefficient
P	Number of pair poles	**J**	Moment of inertia
$\boldsymbol{\omega_m}$	Turbine rotor angular speed	$\boldsymbol{\beta}$	Pitch angle
$\boldsymbol{\omega_{ref}}$	Reference rotor speed	$\boldsymbol{\lambda}$	Tip speed ratio

* Corresponding author: enghady20495@gmail.com

ω_g	Electric angular rotor speed	ρ	Air density (Kg/m3)
C_p	Power coefficient	R	Turbine radius (m)
V_{wind}	Wind speed (m/s)	$V_{ds,qs}$	d–q stator voltage components
A	Turbine blades swept area (m^2)	$i_{ds,qs}$	d–q stator current components

1. INTRODUCTION

The rapid universal demand of electricity increases the using of fossil fuels which have many environmental damages such as pollution and global warming[1, 2]. Therefore, there is an urgent desire to expand the use of renewable energies such as wind, hydro and solar energies which are clean, cheap and with no environmental impacts[3, 4]. Wind energy is one of the most important and commonly used renewable energy resources which is expected to supply about 20% of electricity around the world by 2030[5, 6]. For producing electricity from wind energy, a (WECS) is used which has one of two types wind turbine topology, The first one is the fixed wind turbine (FSWT) and the second type is the variable speed wind turbine[3]. The fixed speed turbine has some drawbacks such as it need multistage gearbox and its speed range is narrow , On The other hand the variable speed wind turbine (VSWT) is commonly used as it can extract The maximum Power at different wind speed Condition and without need of gearbox[3, 6], There are several types of generator can be applied with WECS such as the doubly fed induction generators (DFIGs), squirrel cage induction generators (SCIGs), and the (PMSGs)[7], Although the (DFIGs) can be applied to supply about 25-30% of the active and the reactive power by using partial Converters and the (SCIGs) are simple, cheap and reliable, On the other hand these types of generators have many drawbacks such as high power variation, high mechanical stress and the voltage ride through (VRT) Faults are capable.[8]. For These reasons and for their good characteristics the (PMSGs) are widely used in the WECSs as they have high Power density, high efficiency, and very good Controllability at different wind speed conditions[9, 10]. At the same time the gearbox and the DC excitation system absence increase the generators efficiency by 10% with respect to other types of generators[2, 7]. The WECS based on PMSG is tied to the national power grid through back-to-back (BTBC) converter which consists of the machine side converter (MSC) which is applied to extract the maximum power, the grid side converter(GSC) which is applied to regulate the DC voltage and supply the national grid with an active power at unity power factor and the DC- bus which links the (MSC) and the (GSC)[11, 12] .Many several types of control strategies are applied on the (MSC) to achieve the maximum power point tracking and on the (GSC) to control suppling the power to the national grid. This control stratifies include the conventional PI controller, the fuzzy logic controllers, the sliding mode controller (SMC) and the adaptive neuro fuzzy interface system (ANFIS) controller[13, 14]. in the view of their advantages including simplicity of construction, fast response and ease of gains determination the PI controllers are widely used in the WECSs[3, 15]. It should be highlighted here that the metaheuristic algorithms and optimization approaches are used to determine the optimal PI controller parameter settings[16]. The WECS is susceptible to a variety of abnormal conditions, including three phase symmetrical and unsymmetrical faults, lightning and flicker, and so on[17]. These defects have a negative impact on the WECS, including the three-phase short circuit fault, which causes voltage dips and large currents in the stator windings of the PMSG as well as in the converters' DC-bus voltage[18]. These currents may cause harm to the WECS based on PMSG converters[18, 19]. To avoid the harmful impacts, it is necessary to provide a powerful protection for the WECS socially the PMSG, DC-bus capacitor, and converters[17, 20]. This paper proposes a fresh approach to use the PSO algorithm to comprehensively build the PI controllers of the MSC and the GSC of a grid-linked VSWT-PMSG systems. The maximum power point, the generator reactive power, and the generator currents are all optimally regulated by the PSO-PI controllers by means of the MSC. The PCC voltage, DC link voltage, and grid currents are also effectively controlled by the PSO-PI controllers through the GSC. The firing pulses of the converters' electrical switches are produced by using cascaded or vector control systems in all of these control strategies. The sum of the squared error of these variables represents the objective function, and the PSO is used to minimize it. The range of the proportional and integral gains of the PI controllers is one of the constraints of the optimization issue. (MATLAB/SIMULINK 2015) Software is used to implement all simulation investigations, including the PSO code. The validity of the suggested PSO-PI controllers is examined under various grid disturbances, such as exposing the system to symmetrical and unsymmetrical short circuit faults. This constitutes a significant and novel contribution of this study. The grid-linked VSWT- PMSG's LVRT capability can be further enhanced with the optimal gain PSO-PI controller. The main problem discussed by this paper is how to protect the WECS based on PMSG in the case of grid faults occurrence and how to mitigate the dangerous effects of these faults including the increase in the DC voltage value and the stator currents by setting the PI controllers gains to its optimal values using the PSO algorithm. The remainder of the paper is structured as follows: In Section 2, modelling of the WECS based on PMSG is shown. The PSO algorithm is described in general in Section 3. In Section 4, the employed objective function is described. The optimization and simulation results are discussed in Section 5. The conclusion of this paper is presented in Section 6, which concludes it.

2. THE WECS BASED ON PMSG MODELING

The three-phase WECS based on PMSG is consist of 1.5 MW variable speed wind turbine to provide the mechanical energy which used as a prime mover to a three phase PMSG which is direct connected coupled to the wind turbine[3]. The electrical power generated is supplied to the national power grid through a fully controlled back-to-back converter which consists of the MSC and the GSC connected through a common DC-bus capacitor as shown in Fig.1.[21]. the MSC is applied to maximize the generated power and the GSC is applied to regulate the DC-bus voltage and ensuring suppling the national grid with real power at unity power factor[22].

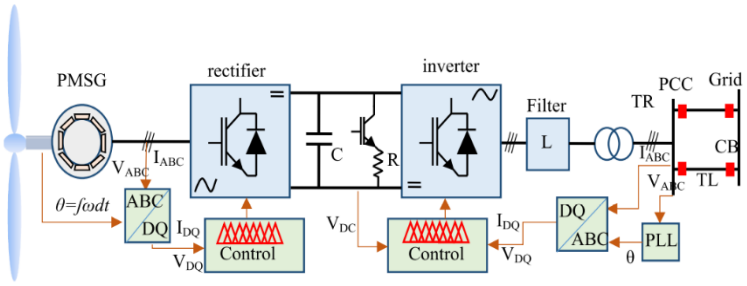

Fig. 1. Standard WECS based on PMSG.

2.1. Wind Turbine modeling

The wind turbine acts as a prime mover for the WECS as it converts the incident kinetic energy of the wind into mechanical power, the input power incident to the wind turbine is expressed as follows[17, 23]:

$$P_{\text{wind}} = \frac{1}{2}\rho A V_{\text{wind}}^3 \tag{1}$$

where ρ donates the air density in (kg/m^3), A donates the swept area of the wind turbine blades in (m2), and V_{wind} represents the velocity of wind in (m/s). The mechanical power Pm produced by the wind turbine is expressed as follows:

$$P_m = C_p(\lambda,\beta)\frac{\rho A}{2}V_{\text{wind}}^3 \tag{2}$$

where C_p represents the power coefficient, β donates the pitch angle of the wind turbine blades, and λ donates the tip speed ratio which represents the relation between the optimal speed and the actual running speed of the wind turbine shaft [24]. From the previous equation it should be highlighted that the aerodynamic performance of the wind turbine is affected by the power coefficient value $C_{\text{p}}(\lambda,\beta)$, which is related with the wind turbine blades pitch angle β and the tip speed ratio λ [25]. The tip speed ratio λ and the power coefficient C_p are formulated as follows with a fixed bitch angle β = 0:

$$\lambda = \frac{\omega_m R}{V_{\text{wind}}} \tag{3}$$

where R stands for the wind turbine blade radius, ω_m stands for the actual rotor speed and V_{wind} stands for the incident wind speed.

$$C_p(\lambda,\beta) = C_1\left(\frac{C_2}{\lambda_i} - C_3\beta - C_4\right)e^{\frac{-C_5}{\lambda_i}} + C_6\lambda \tag{4}$$

where

$$\lambda_i^{-1} = (\lambda + 0.08\beta)^{-1} - 0.035(1+\beta^3)^{-1} \tag{5}$$

Appendix A lists the coefficients of the wind turbine (C1–C6). The captured mechanical power from the variable speed wind turbine is affected by the operating regions that are constrained by cut-in speed ($V_{\text{cut in}}$) and cut-out speed ($V_{\text{cut out}}$), these different regions fall under the following categories as shown in Fig.2.[26].

- In Regions 1 and 4 the wind turbine is forced to be out of service due to the turbine protection[11].
- In Region 2, often known as the maximum power point region, the wind turbine operates below the rated wind speed for the optimal power extraction[1, 10].
- Region 3, the pitch control region: To lessen mechanical stress on the wind turbine blades over the rated wind speed, the pitch controller confines the mechanical power to evaluated power[27].

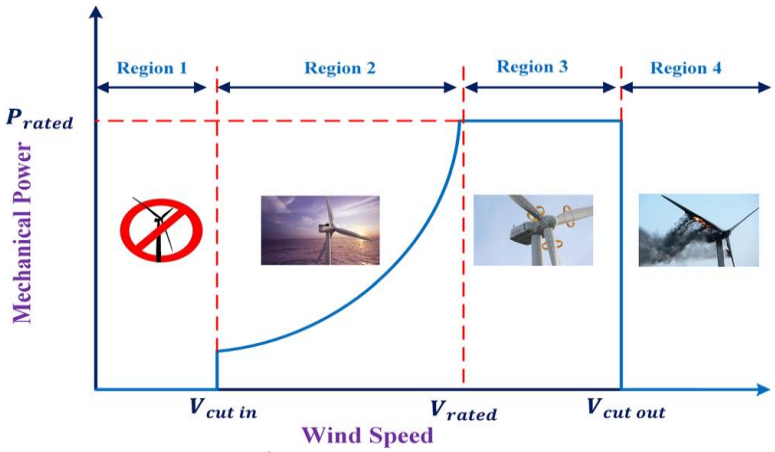

Fig. 2. Operating regions for WECSs (WECS).

2.2. PMSG's modeling

Due to its satisfied power density, affordable pricing, and capability of coupling to the wind turbine without a gearbox at small variations in turbine speed, PMSGs are being employed more and more in the WECSs[3, 7]. The following expressions show the formula of the d-axis and q-axis voltages (V_{ds} and V_{qs}) in the ***dq*** reference frame for a surface-mounted PMSG.

$$V_{ds} = R_s i_{ds} + L_d \frac{di_{ds}}{dt} - \omega_s L_q i_{qs} \tag{6}$$

$$V_{qs} = R_s i_{qs} + L_q \frac{di_{qs}}{dt} + \omega_s L_d i_{ds} + \omega_s \lambda_m \tag{7}$$

where L_d and L_q donate the inductances in the d-q-axis, λ_m donates the linkage flux of the rotor in weber, ω_ss stands for the electrical speed, R_s stands for the resistance of the stator resistance in ohms and i_{ds} and i_{qs} are the stator direct and quadrature axes currents. The following equation can be used to calculate the electromagnetic torque of the PMSM.

$$T = T_{em} + T_r = \frac{3}{2} \cdot \frac{P}{2} \cdot i_{qs}\left[\lambda_m + \left(L_d - L_q\right) \cdot i_{ds}\right] \tag{8}$$

where P is the number of poles and T_r andT_{em}, respectively, are the electromagnetic and the reluctance torques. $L_d = L_q$ for the PMSG that is surface-mounted. $T_r = 0$, and the machine torque is then can be calculated as follow:

$$T = T_{\mathrm{em}} = \frac{3}{2} \cdot \frac{P}{2} \cdot i_{\mathrm{qs}} \lambda_m \tag{9}$$

2.3. Machine side converter

As depicted in Fig. 3, the main function of the MSC is to extract the maximum power possible from the wind turbine at various wind speeds[24]. Operating at the maximum power coefficient, Cp opt=0.48, the wind turbine's output power reaches its maximum value. In order to achieve the maximum power point tracking a controller is employed to control the rotor speed $\boldsymbol{\omega}$m which must be at the MPPT region's limits to obtain the optimal value of the tip speed ratio TSR opt=8.1[28, 29]. When the wind speed exceeds the rated speed, pitch control is utilized to keep the wind turbine running safely at full output power[30]. The control scheme of the MSC consists of two control loops to implement the field-oriented control (FOC) ,the first one is the outer control loop and applied to

regulate the turbine shaft speed to the optimal speed and the second one is the inner control loop witch applied to controls the generator currents with its reference to maximize the developed electromagnetic torque T_{em}, which is related to the quadrature axes current i_{qs} ,here it should be highlighted that the direct axis current $i_{\text{ds}}$is imposed to zero. As well as the inner control loop used to generate the MSC operating pulses[31, 32].

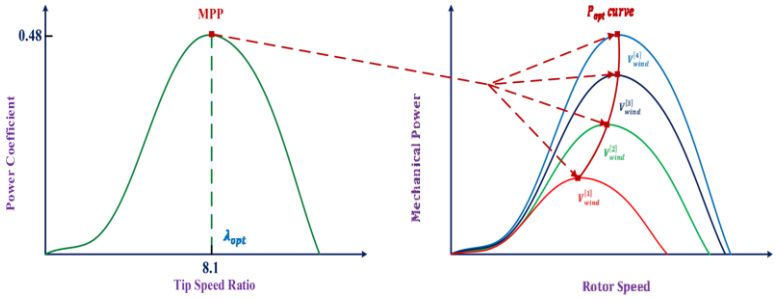

Fig. 3. The wind turbine's power characteristics.

2.4. Grid side converter

To control the DC link voltage and power flow to the national power grid , the GSC with voltage-oriented control (VOC) scheme is applied[11, 32]. Dual control loops are used to establish it; the outer loop controls the DC link voltage, and the inner loop is used to inject active power from the MSC into the national grid at unity power factor to achieve this goal the quadrature current reference, $I_{\text{q-ref}}$ value must be zero[13, 33]. The GSC voltages and the voltages suppling to the grid are calculated as follows:

$$\begin{bmatrix} V_{ia} \\ V_{ib} \\ V_{ic} \end{bmatrix} = [R_f] \begin{bmatrix} i_{fa} \\ i_{fb} \\ i_{fc} \end{bmatrix} + \begin{bmatrix} \dot{\lambda}_a \\ \dot{\lambda}_b \\ \dot{\lambda}_c \end{bmatrix} + \begin{bmatrix} V_{ga} \\ V_{gb} \\ V_{gc} \end{bmatrix} \tag{10}$$

Where R_f and L_f represent the diagonal matrices, $\dot{\lambda}_a = L_f \frac{\mathrm{d}i_{fa}}{\mathrm{d}t}, \dot{\lambda}_b = L_f \frac{\mathrm{d}i_{fb}}{\mathrm{d}t}$ and $\dot{\lambda}_c = L_f \frac{\mathrm{d}i_{cc}}{\mathrm{d}t}$

$$\begin{bmatrix} V_{id} \\ V_{iq} \end{bmatrix} = [r_f] \begin{bmatrix} i_{fd} \\ i_{fq} \end{bmatrix} + \begin{bmatrix} \dot{\lambda}_{fd} - \omega_g \psi_{fq} \\ \dot{\lambda}_{fq} + \omega_g \psi_{fd} \end{bmatrix} + \begin{bmatrix} V_{gd} \\ V_{gq} \end{bmatrix} \tag{11}$$

where $\omega_g = 2\pi f_g, \psi_{fq} = l_f i_{fq}, \psi_{fd} = l_f i_{fd}, \dot{\lambda}_{fd} = l_f \frac{\mathrm{d}}{\mathrm{d}t} i_{fd},, \dot{\lambda}_{fq} = l_f \frac{\mathrm{d}}{\mathrm{d}t} i_{fq}$.The reactive power supplied to the national grid through the MSC is canceled by setting the grid quadrature voltage component V_{gq} value to zero, as a result only active power with power factor equals to 1 is injected to the national grid[13]. The outer PI control loop controls the DC link capacitor voltage by suppling the capacitor current reference value I_c which is represented as follows[10]:

$$I_c = \frac{P_e - P_g}{V_{\text{dc}}} = C \frac{\mathrm{d}V_{\text{dc}}}{\mathrm{d}t} \tag{12}$$

where P_e stands for the output power of the MSC and P_g stands for the GSC active power supplied to the grid. The capacitance and voltage of the DC-bus capacitor are donated respectively by C and V_{dc}.So the reference value of the quadrature axis component of the capacitor current i_{fd}^* is calculated as follows:

$$i_{fd}^* = I_s - I_c^* \tag{13}$$

where I_s is the MSC current witch is calculated as follows:

$$I_s = \frac{P_e}{V_{\text{dc}}} \tag{14}$$

Finally, the following expressions stand for the active powerP_g and the reactive power components supplied to the national power grid through the GSC:

$$P_g = \frac{3}{2} V_{gd} i_{fd} \tag{15}$$

$$Q_g = \frac{3}{2} V_{gd} i_{fq} \tag{16}$$

3. THE PARTICLE SWARM OPTIMIZATION TECHNIQUE (PSO)

Kennedy and Eberhart invented Particle Swarm Optimization, a meta-heuristic optimization technique in 1995[16]. The PSO algorithm may solve both continuous and binary or discrete problems. This meta-heuristic, on the other hand, appears to function best in domains with continuous variables[34, 35]. A swarm is randomly distributed in the dimension of the search space D, and each particle is randomly placed in the location Xi of the search space; each particle also has a random speed[35]. The change in speed is a simple linear mixture of three trends: its own present speed, its own experience, and the trend toward improved swarm performance[36]. The equations describe the update of two vectors including the speed and the position of each particle in the swarm are expressed as follow.

$$\begin{cases} V_{iD}^{t+1} = k \times V_{iD}^{t} + c_1 r_1 (P_{iD}^{t} - x_{iD}^{t}) + c_2 r_2 (G_{iD}^{t} - x_{iD}^{t}) \\ x_{iD}^{t+1} = V_{iD}^{t+1} + x_{iD}^{t} \end{cases} \tag{17}$$

where *I* equals 1,2,3,4,...,n,, while n donates the swarm size, D donates the search space dimension, c1 and c_2 represent the positive constants, k donates the momentum of inertia, r_1 and r_2 represent random numbers which are uniformly distributed in [0, 1, The iteration number is determined by t, P donates the i^{th} particle's best previous position (the position with the highest fitness value), and G donates the best particle in the swarm. First, a random swarm population with random vector locations (x) and velocity vectors (V!) is produced. Each particle fitness value is calculated to investigate the present position of particles and compare it to the fitness value of other swarms[37]. If the particle's present position is better than its best previously attained position, the particle's experience is altered. Furthermore, a particle's velocity is changed based on the global best particle and its bests own experience[37, 38]. In reality, particles in each iteration migrate toward the best global particle. Finally, the best global particle is updated, as shown in Fig.4. To speed up the PSO convergence, it was recommended to discover a better solution with the least period of calculation time and accuracy[39]. The best solution is calculated by minimizing a certain criterion (objective function), which is the mean square error (MSE) derived by the following equation.

$$\text{MSE} = \text{Fitness} = \frac{1}{nT} \sum_{i=1}^{n} e(K)^2 \tag{18}$$

where: the total samples number is donated by e(k) and T represents the sampling time.

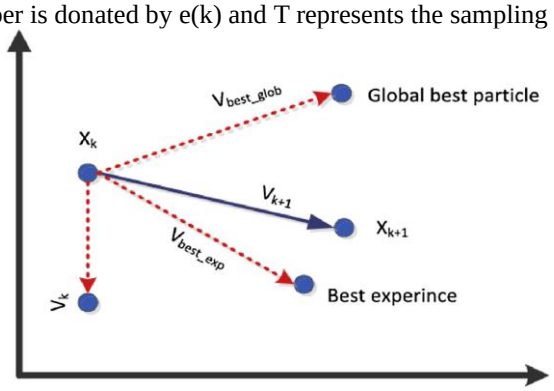

Fig. 4. Dynamic of swarms in particle swarm optimization.

4. THE OBJECTIVE FUNCTION

The main target of this study is to enhance the grid-linked WECS based on PMSG low voltage ride-through capability. By adjusting the PI controllers gains of for the control system to their optimal values, this goal can be accomplished. The power system, however, is a sizable nonlinear dynamic system that cannot be modelled by a

transfer function, as illustrated in Fig. 1. As a result, the objective function is defined as the integral sum of the squared errors of the PI controllers as expressed in 19. In this study, the objective function is minimized using the PSO algorithms.

$$\begin{aligned} \text{ISE}\ (x_1, x_2, \dots, x_8) = \int_0^4 \Big[\left(P_{max} - P_g\right)^2 + \left(Q_{ref} - Q_g\right)^2 + (V_{dc}^* - V_{dc})^2 \\ +(V_{rms}^* - V_{rms})^2 + \left(i_q^* - i_q\right)^2 + (i_d^* - i_d)^2 + \left(i_{gd}^* - i_{gd}\right)^2 + \left(i_{gq}^* - i_{gq}\right)^2 \Big] dt \end{aligned} \quad (19)$$

where $x_1, x_2, \dots, x_8$ represent the values of the PI controllers gains, V_{dc} is the voltage of the DC-bus, $P_{max}\ and\ P_g$ represent the maximum and generated active power ,respectively, $Q_{ref}\ and\ Q_g$ represent the reference and generated reactive power ,respectably, $i_q^*\ and\ i_q$ donate the PMSG stator reference and actual quadrature axis currents, respectively,, $i_d^*\ and\ i_d$ donate the PMSG stator reference and actual direct axis currents, respectively, $i_{gq}^*\ and\ i_{gq}$ donate the reference and the actual value of the grid side quadrature axis currents, respectively,, $i_d^*\ and\ i_d$ donate the grid side reference and actual direct axis currents, respectively while $V_{rms}^*and\ V_{rms}$ are the grid side reference and actual voltages, respectively .

5. SIMULATION RESULTS AND DISCUSSION

The state simulation results were obtained using MATLAB/SIMULINK (MATLAB 2015) in order to study the performance of the investigated system under the three phase to ground short circuit fault and to enhance the system performance by mitigating the dangerous effects of the fault by adjusting the gains of the PI controllers used in the system to the optimal values with the using of the PSO optimization technique. the WECS based on PMSG parameters of the system under study are listed in Appendix 1.

5.1. Optimization Results

The PSO poetization technique is employed to obtain the optimal gains for the PI controllers by minimizing the objective function expressed in Equation (23). To determine the optimal PI controllers' gains, the PSO algorithms are coded and implemented in MATLAB/SIMULINK software. The parameters of the PSO optimization technique are listed in Table 1, where the number of optimization iterations for each algorithm is 150 and the simulation time for each iteration is 4 seconds. Furthermore, the balanced fault is taken into account during optimization in order to emphasis improving the low voltage ride-through (LVRT) capability of the WECS based on PMSG connected to the national grid. Fig. 8 depicts the convergence curves of the integral squared-error (ISE) minimization using the PSO optimizer, with Table 2. displaying the optimal 8 variables of the four PI controllers which are optimally designed based on the PSO optimizer.

TABLE 1. THE PSO OPTIMIZER PARAMETERS.

Parameters	Values
Population Size (Swarm Size)	*15*
Maximum Number of Iterations	*50*
Inertia weight factor (w)	*1*
Confidence coefficient	*c_1 =1.5 and c_2 =2*
Inertia Weight Damping Ratio	0.99

TABLE 2. THE OPTIMAL VALUES OF THE PI CONTROLLERS' GAINS.

PI number	Parameters	Values
PI_1	K_p	*0.0813*
	K_i	*0.9866*
PI_2	K_p	*0.0847*
	K_i	*1.3697*
PI_3	K_p	*60.9874*
	K_i	*418.0504*
PI_4	K_p	*1.4025*
	K_i	*23.3271*

5.2. Simulation Results

This section presents the WECS based on PMSG performance under grid short circuit faults ,as the study based on two cases, in the first case the fault simulated is a three phases to ground short circuit fault which represents

balanced short circuit faults while in the second case the simulated fault is a line to line short circuit fault which represents balanced short circuit faults, also this section shows the vital role of setting the PI controllers' gains to their optimal values in mitigating the dangerous effects of the grid short circuit faults.

- **Case 1, The WECS based on PMSG performance under three phase to ground short circuit fault**

A three phase to ground short circuit fault is simulated to be occurred across the grid side terminal for 150 m Sec. This signifies that the three-phase lines of TL are short-circuited with ground. As shown in Fig. 1, this fault occurs at the Point of common coupling (PCC) bus bar at the end of one circuit of the double-circuit TLs. The simulating time is 4 Sec., and the fault occurs at time T= 3 Sec. and lasted to T=3.15 Sec., after that the circuit breakers (CBs) trip so the fault is cleared.

Because of the excessive power in the DC -bus, the DC -bus voltage rises during the fault, resulting in an unfavorable overvoltage across the DC capacitors, which can be damaged. Chopper circuits are used to protect these capacitors, as seen in Fig. 1. The control system also adjusts the DC voltage across the capacitors. In case of the three phase to ground fault and without setting the PI controllers' gains to their optimal values the DC-bus voltage increases to 1500 V, this very high DC voltage can damage the DC-bus capacitor and the WECS converters on the other hand the value of the DC-bus voltage during the fault drops back to its rated value (1150 V) with setting the PI controllers' gains to their optimal values as shown in Fig. 5.

Fig. 6. displays the real power response during the three phase to ground fault, which drops to 0.5 p.u. during the fault at PCC without setting the PI controllers' gains to their optimal values while during the fault and with the PI controllers' gains are set to their optimal values the active power rises to 0. 75p.u which is close to the. steady state value.

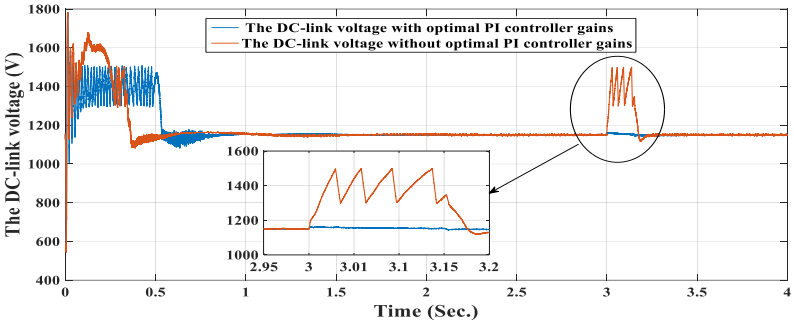

Fig. 5. The DC- bus voltage with and without optimal PI controllers' gains.

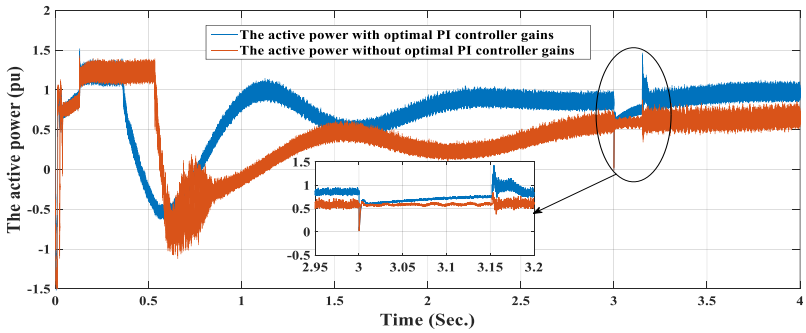

Fig. 6. The Active Power with and without optimal PI controllers' gains.

For a unity power factor correction, the reactive power at PCC should be very close to zero at steady state. After fault clearance, the GSC provides reactive power to the grid to restore grid stability. The reactive power supplied by the WECS based on PMSG to the grid during the fault and without setting the PI controllers' gains to their optimal values reaches to -0.5 p.u. which means that the WECS based on PMSG consumes reactive power from the grid, in the case of setting the PI controllers' gains to their optimal values and during the fault the reactive power value rises to about -0.6 p.u. as shown in Fig. 7.,it should be highlighted here that the value of the reactive power after clearing the fault with optimal PI controllers' gains (0.5 p.u.) is better than that without optimal PI controllers' gains (1.4 p.u.)as the high value of the reactive power supplied to the grid after clearing the faults can lead to grid instability.

As depicted in Fig. 8. The electromagnetic torque profile during the fault is enhanced with the PI controller gain are set to their optimal values compared with it in the case of using the PI controller without optimal gains.

When a three phase to ground grid fault occurs, the PMSG stator voltage and current are affected. Fig. 9. (a) illustrates that the stator voltage rises to 3.2 p. u during the fault occurrence and without setting the PI controllers'

gains to their optimal values When the PI controllers' gains are set to their optimal values the stator voltage value reduces back to its rated value, as shown in Fig.9 (b).

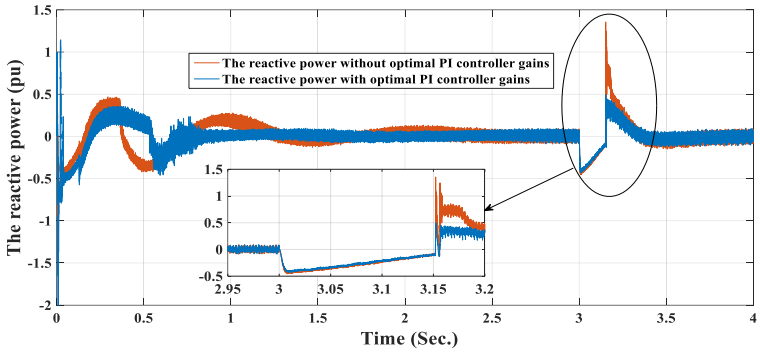

Fig. 7. The Reactive Power with and without optimal PI controllers' gains.

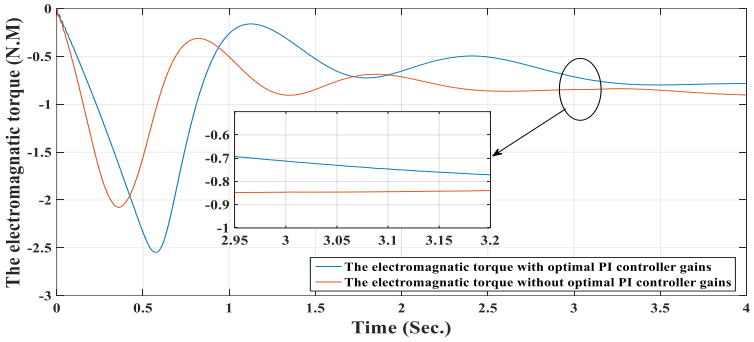

Fig. 8. The Electromagnetic torque with and without optimal PI controllers' gains.

At the same time, the stator current increases during the fault and without setting the PI controllers' gains to their optimal values as shown in Fig.10 (a). In contrast, as shown in Fig.10, (b). using the PI controller with optimal gains during the three phase to ground fault limits the stator current to its rated value.

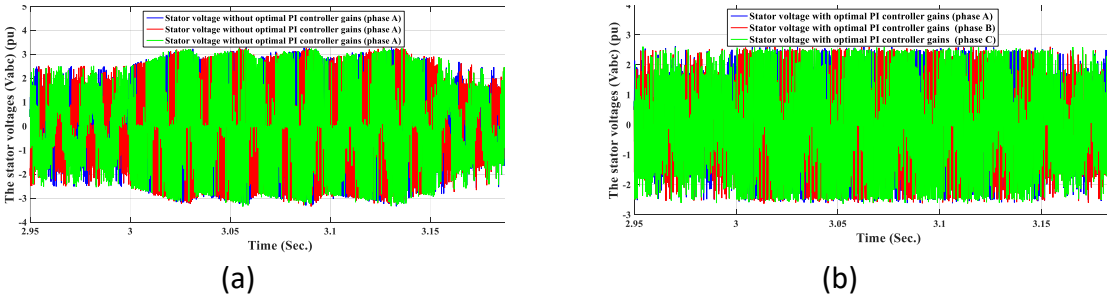

Fig. 9. Stator voltage (a) Without optimal PI controllers' gains., (b) With optimal PI controllers' gains.

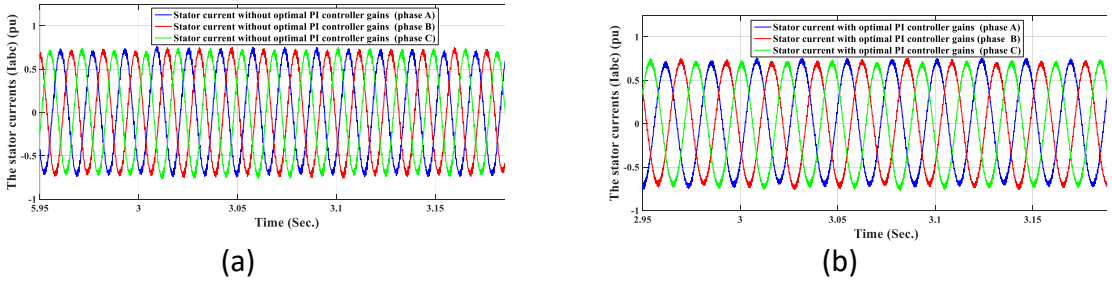

Fig. 10. The stator current (a) Without optimal PI controllers' gains., (b) With optimal PI controllers' gains.

- **Case 2, The WECS based on PMSG performance under line-to-line short circuit fault**

A 150 m Sec. line-to-line short circuit fault is simulated over the grid side terminal. This indicates that two lines of the TL are short-circuited, and the fault occurs at the PCC bus bar at the end of one circuit of the double-circuit TLs. The simulation time is 4 Sec., and the fault started at time T=3 Sec. and lasted until T=3.15 Sec., at this point the circuit breakers (CBs) tripped, clearing the fault.

The DC-bus voltage rises to 1550 V in the case of a line-to-line fault when the PI controllers' gains are not set to their optimum values. This extremely high DC voltage can harm the WECS converters and the DC-bus capacitor. On the other hand, the DC-bus voltage during the fault falls back to its rated value (1150 V) when the PI controllers' gains are set to their optimum values, as shown in Fig. 11

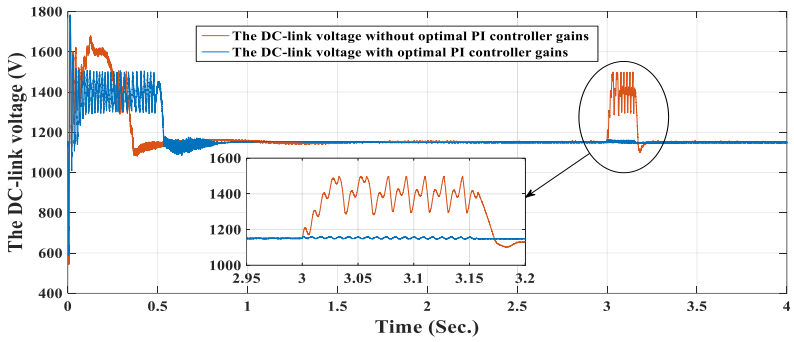

Fig. 11. The DC- bus voltage with and without optimal PI controllers' gains.

Fig.12. shows the active power response during the line-to-line fault, which oscillates between 0 p.u. and 1.3 p.u. during the fault at PCC without setting the PI controllers' gains to their optimal values. However, during the fault and with the PI controllers' gains set to their optimal values, the active power oscillations are damped to oscillate between 0.5 p.u. and 0.9 p.u., which can enhance the active power profile during the fault.

As illustrated in Fig.13, the reactive power value is reduced to fluctuate between -0.5 and 0.45 p.u. when the PI controllers' gains are set to their optimal settings and when the fault is present. With respect to its value during the fault and without adjusting the PI controllers' gains to their optimal values as in this case the reactive power delivered to the grid by the WECS based on PMSG oscillates between -0.7 p.u. and 0.7 p.u.

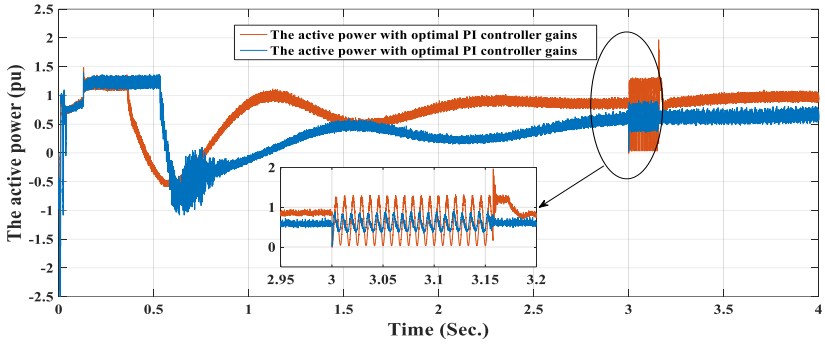

Fig. 12. The Active Power with and without optimal PI controllers' gains.

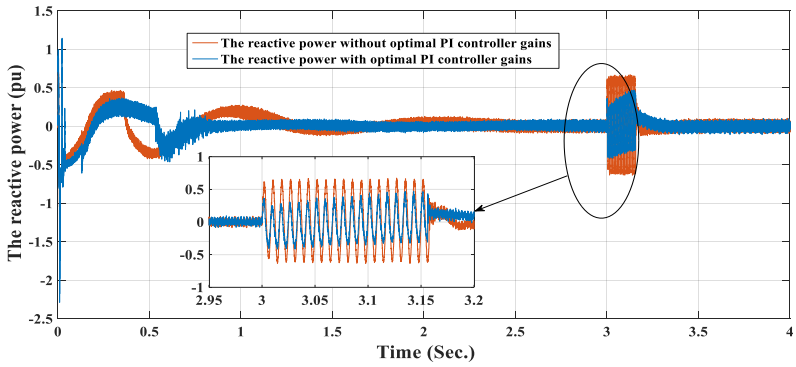

Fig. 13. The Reactive Power with and without optimal PI controllers' gains.

As illustrated in Fig. 14. When the PI controllers' gains are set to their optimal levels compared to when utilizing the PI controller without optimal gains, the electromagnetic torque profile is improved during the fault.

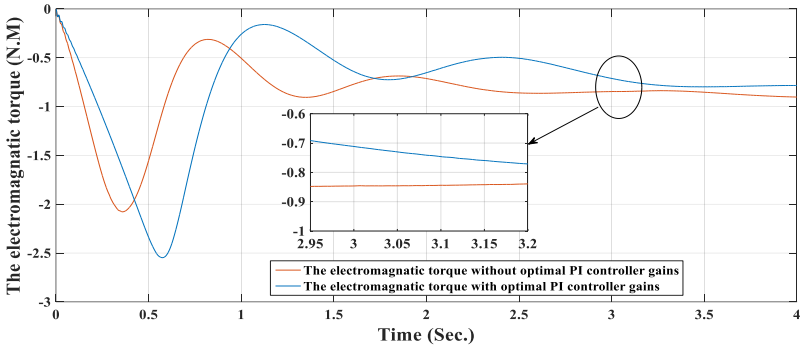

Fig. 14. The Electromagnetic torque with and without optimal PI controllers' gains.

The PMSG stator voltage and current are impacted by the line-to-line grid fault occurrence. Fig. 15. (a) shows that during the occurrence of the fault and without setting the PI controllers' gains to their optimal settings, the stator voltage increases to 3.3 p.u. The stator voltage value decreases back to its rated value when the PI controllers' gains are set to their optimal levels, as depicted in Fig.15. (b). While the fault is occurring and without optimizing the PI controllers' gains as illustrated in Fig. 16. (a)., the stator current also increases. Contrarily, as depicted in Fig.16 (b). When a line-to-line fault occurs, utilizing the PI controller with the optimal gains restricts the stator current to its nominal value.

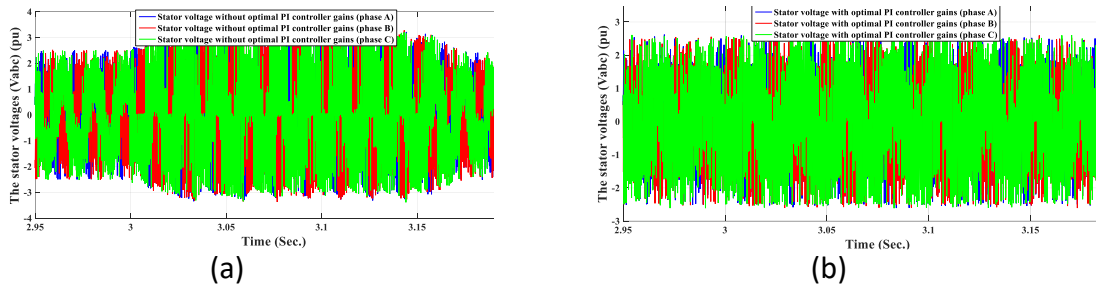

Fig. 15. Stator voltage (a) Without optimal PI controllers' gains., (b) With optimal PI controllers' gains.

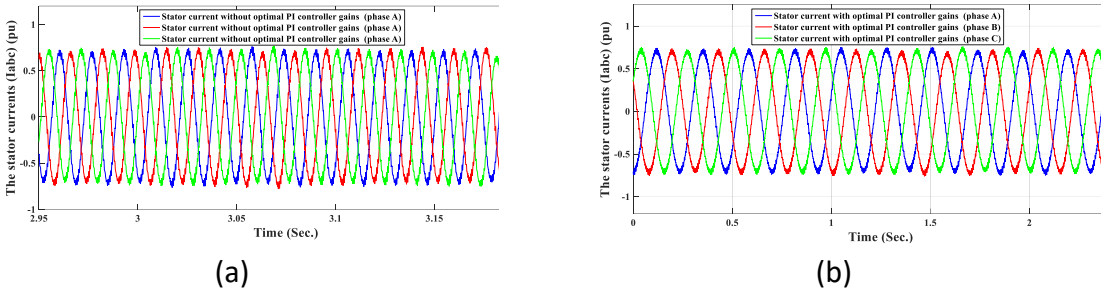

Fig. 16. The stator current (a) Without optimal PI controllers' gains., (b) With optimal PI controllers' gains.

6. CONCLUSION

This paper has depicted the performance of the WECS-based PMSG in this work with and without setting the gains of the system PI controllers to the optimal values The performance was investigated for 150 m sec under two types of short circuit faults: the three phase to ground short circuit fault as an example of balanced short circuit faults and the line-to-line short circuit fault as an example of unbalanced short circuit faults without setting the gains of the system PI controllers to the optimal values. The appropriate optimal values of the PI controllers' gains for the two types of faults were then determined using the efficient PSO optimizer to protect the WECS-based PMSG system. The obtained results confirmed that setting the gains of the system PI controllers optimally may decrease the stator currents to the permitted limits significantly improved the performance of the WECS-based PMSG under faults. Furthermore, the DC voltage was dropped and the reactive power was boosted to its reference value when the PI controllers' gains were not set to the optimal values. In addition, the active power

profile was improved. As shown above the paper results helps to protect the WECS based on PMSG form damages and dangerous effects could be happened during and after grid faults accordance. this also will help to save the sustainability of WECS based on PMSG with the power grid and avoid the WECS based on PMSG disconnecting during and after grid faults occurrence. In the other hand and as a result of these noteworthy and admirable accomplishments, researchers will be inspired to employ the PSO-PI controllers to improve the performance of numerous systems, including renewable energy systems, microgrids, and smart grid systems.

Appendix A

A.1 Specification of wind turbine Parameters	Values	
The coefficients C_1 to C_6	C_1= 0:5176	C_4=5
	C_2=116	C_5= 21
	C_3=0:4	C_6=0:0068
Blade radius	R_b = 35:25 m	
Air density	ρ_{air} = 1:225 kg/m^3	
Optimal tip speed ratio	λ_{max} = 8.1	
Maximum Power Coefficient	$C_{p\,max}$ = 0.48	

A.2. Three-phase PMSG parameters Parameters	Values
Rated power	P =1:5 MW
Pole pairs number	n_p =40
Stator resistance	R_s = 3:17 m ohm
Stator inductance	L_s = 3:07 mH
Moment of inertia	J =10000 kg/m^2
Flux linkage	ψ= 7:0172 wb

A.3. DC bus and gird parameters Parameters	Values
Dc-link voltage	Vdc =1150V
Capacitor of the dc-link	C =0:023 F
Grid voltage	V_g =575 V
Grid frequency	F =60 Hz
Grid resistance	R_g =0:003 p.u.
Grid inductance	L_g =0:3 p.u.

7. REFERENCES

[1] Mousa, H.H.H., A.R. Youssef, And E.E.M. Mohamed, Study of Robust Adaptive Step-Sizes P&O MPPT Algorithm for High-Inertia WT With Direct-Driven Multiphase PMSG. International Transactions on Electrical Energy Systems, 2019. 29(10).

[2] Belkhier, Y., Et Al., Modified Passivity-Based Current Controller Design of Permanent Magnet Synchronous Generator for Wind Conversion System. International Journal of Modelling And Simulation, 2020. 42(2): P. 192-202.

[3] Qais, M.H., H.M. Hasanien, And S. Alghuwainem, Optimal Transient Search Algorithm-Based PI Controllers for Enhancing Low Voltage Ride-Through Ability of Grid-Linked PMSG-Based Wind Turbine. Electronics, 2020. 9(11).

[4] Soliman, M.A., Et Al., An Adaptive Fuzzy Logic Control Strategy for Performance Enhancement of A Grid-Connected PMSG-Based Wind Turbine. IEEE Transactions On Industrial Informatics, 2019. 15(6): P. 3163-3173.

[5] Mousa, H.H.H., A.-R. Youssef, And E.E.M. Mohamed, Optimal Power Extraction Control Schemes for Five-Phase PMSG Based Wind Generation Systems. Engineering Science And Technology, An International Journal, 2020. 23(1): P. 144-155.

[6] Mousa, H.H.H., A.-R. Youssef, And E.E.M. Mohamed, Hybrid and Adaptive Sectors P&O MPPT Algorithm Based Wind Generation System. Renewable Energy, 2020. 145: P. 1412-1429.

[7] Okedu, K.E. And S.M. Muyeen, Enhanced Performance of PMSG Wind Turbines During Grid Disturbance at Different Network Strengths Considering Fault Current Limiter. International Transactions on Electrical Energy Systems, 2021. 31(8).

[8] Mousa, H.H.H., A.-R. Youssef, And E.E.M. Mohamed, Adaptive P&O MPPT Algorithm Based Wind Generation System Using Realistic Wind Fluctuations. International Journal of Electrical Power & Energy Systems, 2019. 112: P. 294-308.

[9] Saidi, Y., Et Al., A Comprehensive Review of LVRT Capability and Advanced Nonlinear Backstepping Control of Grid-Connected Wind-Turbine-Driven Permanent Magnet Synchronous Generator During Voltage Dips. Journal of Control, Automation and Electrical Systems, 2022. 33(6): P. 1773-1791.

[10] Mousa, H.H.H., A.-R. Youssef, and E.E.M. Mohamed, Variable Step Size P&O MPPT Algorithm for Optimal Power Extraction of Multi-Phase PMSG Based Wind Generation System. International Journal of Electrical Power & Energy Systems, 2019. 108: P. 218-231.

[11] Mousa, H.H.H., A.-R. Youssef, And E.E.M. Mohamed, Modified P&O MPPT Algorithm for Optimal Power Extraction of Five-Phase PMSG Based Wind Generation System. SN Applied Sciences, 2019. 1(8).

[12] Ramadan, H., Et Al., An Efficient Variable-Step P&O Maximum Power Point Tracking Technique for Grid-Connected WECS. SN Applied Sciences, 2019. 1(12).

[13] Mousa, H.H., A.R. Youssef, And E.E.J.I.T.O.E.E.S. Mohamed, Model Predictive Speed Control of Five-Phase Permanent Magnet Synchronous Generator-Based Wind Generation System Via Wind-Speed Estimation. 2019. 29(5): P. E2826.

[14] Jahanpour-Dehkordi, M., S. Vaez-Zadeh, and J.J.I.T.O.E.C. Mohammadi, Development of A Combined Control System to Improve The Performance of A PMSG-Based WECS Under Normal and Grid Fault Conditions. 2019. 34(3): P. 1287-1295.

[15] Tripathi, S.M., A.N. Tiwari, and D.J.I.T.O.E.E.S. Singh, Optimum Design of Proportional-Integral Controllers in Grid-Integrated PMSG-Based WECS. 2016. 26(5): P. 1006-1031.

[16] Mahmoud, M.M., M.M. Aly, and A.-M.M.J.S.A.S. Abdel-Rahim, Enhancing the Dynamic Performance of A Wind-Driven PMSG Implementing Different Optimization Techniques. 2020. 2(4): P. 1-19.

[17] Errami, Y., M. Ouassaid, and M.J.E.P. Maaroufi, Control of A PMSG Based Wind Energy Generation System for Power Maximization and Grid Fault Conditions. 2013. 42: P. 220-229.

[18] Geng, H., L. Liu, And R.J.I.T.O.S.E. Li, Synchronization and Reactive Current Support of PMSG-Based Wind Farm During Severe Grid Fault. 2018. 9(4): P. 1596-1604.

[19] Zhou, S., Et Al. Improved DC-Link Voltage Control of PMSG WECS Based on Feedback Linearization Under Grid Faults. In 2013 Twenty-Eighth Annual IEEE Applied Power Electronics Conference and Exposition (APEC). 2013. IEEE.

[20] Dey, P., M. Datta, And N. Fernando. A Coordinated Control of Grid Connected PMSG Based WECS Under Grid Faults.in 2017 IEEE 3rd International Future Energy Electronics Conference and ECCE Asia (IFEEC 2017-ECCE Asia). 2017. IEEE.

[21] Jain, A., S. Shankar, and V.J.J.O.G.E. Vanitha, Power Generation Using Permanent Magnet Synchronous Generator (PMSG) Based Variable Speed WECS (WECS): An Overview. 2017. 7(4): P. 477-504.

[22] Ramadan, H., Et Al., An Efficient Variable-Step P&O Maximum Power Point Tracking Technique for Grid-Connected WECS. 2019. 1(12): P. 1-15.

[23] Errami, Y., Et Al., Sliding Mode Control Scheme of Variable Speed WECS Based on The PMSG for Utility Network Connection, in Advances and Applications In Sliding Mode Control Systems. 2015, Springer. P. 167-200.

[24] Baran, J. And A.J.E. Jąderko, An MPPT Control of A PMSG-Based WECS With Disturbance Compensation and Wind Speed Estimation. 2020. 13(23): P. 6344.

[25] Tounsi, A., Et Al. MPPT Algorithm for WECS Based on PMSG. In 2017 18th International Conference on Sciences And Techniques of Automatic Control and Computer Engineering (STA). 2017. IEEE.

[26] Tiwari, R. And N.R.J.I.-P. Babu, Fuzzy Logic Based MPPT for Permanent Magnet Synchronous Generator in WECS. 2016. 49(1): P. 462-467.

[27] Zebraoui, O. And M. Bouzi. Comparative Study of Different MPPT Methods for WECS. In IOP Conference Series: Earth and Environmental Science. 2018. IOP Publishing.

[28] Wang, X., S. Yuvarajan, And L. Fan. MPPT Control for A PMSG-Based Grid-Tied Wind Generation System. In North American Power Symposium 2010. 2010. IEEE.

[29] Sahin, P., R. Resmi, And V. Vanitha. PMSG Based Standalone Wind Electric Conversion System With MPPT. In 2016 International Conference on Emerging Technological Trends (ICETT). 2016. IEEE.

[30] Chen, J., Et Al., Design of Robust MPPT Controller for Grid-Connected PMSG-Based Wind Turbine Via Perturbation Observation Based Nonlinear Adaptive Control. 2019. 134: P. 478-495.

[31] Rezaei, N., Et Al., A Model-Based Implementation of An MPPT Technique and a Control System for A Variable Speed Wind Turbine PMSG. 2019. 31(1): P. 3-15.

[32] Hu, L., Et Al., Sliding Mode Extremum Seeking Control Based on Improved Invasive Weed Optimization for MPPT in WECS. 2019. 248: P. 567-575.

[33] Aubrée, R., Et Al., Design of an Efficient Small Wind-Energy Conversion System With an Adaptive Sensorless MPPT Strategy. 2016. 86: P. 280-291.

[34] Mahmoud, M.M., Et Al., Dynamic Evaluation of Optimization Techniques–Based Proportional–Integral Controller for Wind-Driven Permanent Magnet Synchronous Generator. 2021. 45(3): P. 696-709.

[35] Soufi, Y., S. Kahla, And M. Bechouat, Feedback Linearization Control Based Particle Swarm Optimization for Maximum Power Point Tracking of Wind Turbine Equipped by PMSG Connected to The Grid. International Journal of Hydrogen Energy, 2016. 41(45): P. 20950-20955.

[36] Saad, N.H., A.A. El-Sattar, And M.E.J.A.S.E.J. Marei, Improved Bacterial Foraging Optimization for Grid Connected WECS Based PMSG With Matrix Converter. 2018. 9(4): P. 2183-2193.

[37] Ram, G.N., Et Al., A Novel Maximum Power Point Tracking System for Wind-Energy-Conversion System Using Particle Swarm Optimization. 2014.

[38] Qais, M.H., Et Al. Output Power Smoothing of Grid-Tied PMSG-Based Variable Speed Wind Turbine Using Optimal Controlled SMES. In 2019 54th International Universities Power Engineering Conference (UPEC). 2019. IEEE.

[39] Yang, B., Et Al., Dynamic Leader Based Collective Intelligence for Maximum Power Point Tracking Of PV Systems Affected By Partial Shading Condition. 2019. 179: P. 286-303.